

Bond electronic polarization induced by spin

Chenglong Jia,¹ Shigeki Onoda,² Naoto Nagaosa,^{2,3,4} and Jung Hoon Han^{1,5,*}

¹*Department of Physics and Institute for Basic Science Research,
Sungkyunkwan University, Suwon 440-746, Korea*

²*Spin Superstructure Project, ERATO, Japan Science and Technology Agency,
c/o Department of Applied Physics, University of Tokyo, Tokyo 113-8656, Japan*

³*CREST, Department of Applied Physics, University of Tokyo, Tokyo 113-8656, Japan*

⁴*Correlated Electron Research Center, National Institute of Advanced
Industrial Science and Technology, Tsukuba, Ibaraki 305-8562, Japan*

⁵*CSCMR, Seoul National University, Seoul 151-747, Korea*

(Dated: May 25, 2019)

We study theoretically the electric polarization induced by noncollinear spin configurations in the limit of strong Hund coupling. We employ a model of two magnetic ions sandwitching an oxygen ion. It is shown that there appears a longitudinal polarization P_x along the bond, which is roughly proportional to $(m_r^x)^2 - (m_l^x)^2$ where $m_{r(l)}^x$ is the x -component of the spin orientation vector at right (left) magnetic ion. A numerical study of the model Hamiltonian yields both longitudinal and transverse electric dipole moments. The transverse polarization is shown to have a non-uniform as well as a uniform component, with the latter being consistent with the previous theory. The longitudinal polarization is non-uniform and oscillating with the period half that of the spin order, but the local magnitude is typically much larger than the uniform transverse polarization and may be detected by X-ray/neutron scattering experiments.

PACS numbers: 75.80.+q, 71.70.Ej, 77.80.-e

I. INTRODUCTION

A number of recent experimental breakthroughs has revived interests in the phenomena of coupling of magnetic and electric (dipolar) degrees of freedom in a class of materials known as “multiferroics”^{1–7}. Some noteworthy observations include the development of dipole moments accompanying the collinear-to-helical spin ordering^{3,4,6,7} and adiabatic control of dipole moments through sweeping of applied magnetic fields^{1,2}, which all unambiguously point to the strong coupling of electric and magnetic degrees of freedom in these compounds. A number of phenomenological^{8,9} and microscopic^{10,11} theories has been advanced to establish the connection between non-collinear spin order and ferroelectricity.

In particular the work of Katsura, Nagaosa, and Balatsky (KNB)¹⁰ proposed a microscopic theory for the interplay between non-collinear magnetic order and the dipolar polarization of the electronic wave function induced by it. The magnetic (M) ion is modeled by three degenerate t_{2g} levels experiencing some external magnetic field (to guarantee magnetic order) and subject to spin-orbit coupling. Two such magnetic ions are bridged by an intermediate oxygen (O) atom which itself has no spin-orbit interaction. Solving the model Hamiltonian perturbatively in the M-O hybridization amplitude, KNB finds an electronic polarization orthogonal to the M-O-M axis in the ground states of one and two holes.

In this paper we re-visit the M-O-M cluster model of KNB, but in the different limit of a strong Hund coupling. The M-O-M model in this limit is exactly solvable in the absence of spin-orbit coupling, with two classes of degenerate eigenstates. For these states there is no net

electric polarization. The spin-orbit coupling on the magnetic sites is then introduced as a perturbation within each degenerate manifold. The problem is exactly solvable again and we can calculate the polarization $\langle \mathbf{r} \rangle$ for each of the eigenstates thus obtained. It is shown that *a non-zero polarization develops along the direction of the M-O-M cluster*. We denote such polarization as “longitudinal”, to distinguish it from the “transverse” polarization, perpendicular to the cluster axis, obtained in previous theories^{8,10,11}.

Numerical study of the mean-field Hamiltonian for the cluster confirms the existence of longitudinal polarization predicted analytically, and reveals a non-uniform component in the transverse polarization which is unexpected in previous theories^{8,10,11}. Namely, oscillating components appear in both the longitudinal and transverse polarizations with a vanishing macroscopic average whereas the polarization predicted by existing theories gives a “uniform” component induced by a non-collinear spin order.

This paper is organized as follows. In Sec. II, we introduce the mean-field Hamiltonian for the three-site cluster, and in the limit of a large Hund coupling, its approximate eigenstates are derived analytically in a perturbation theory with respect to the spin-orbit interaction. Up to the zeroth-order in the spin-orbit coupling, electric polarization is then calculated for these eigenstates. In Sec. III, numerical solution of the mean-field Hamiltonian is presented. Fourier analysis of the polarization reveals the existence of both uniform and non-uniform components in the transverse part, and non-uniform component in the longitudinal part. We conclude with a discussion in Sec. IV.

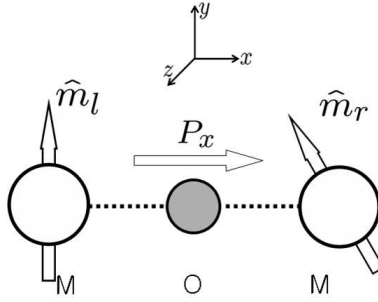


FIG. 1: Arrangement of two magnetic ions and an oxygen atom in the M-O-M cluster. \hat{m}_l and \hat{m}_r are the magnetic moment orientations of the magnetic sites bridged to the intervening oxygen atom. Polarization P_x along the cluster's axis is found (see text for details).

II. EFFECTIVE THEORY

As a minimal unit giving rise to spin-polarization coupling KNB introduced the model shown in Fig. 1. To guarantee that a net average magnetic moment exists, each magnetic site is subject to a spin polarization field¹⁰

$$H_M = -U \sum_{a=l,r} \hat{m}_a \cdot \left(\sum_{b=xy,yz,zx} \mathbf{S}_{a,b} \right) \quad (1)$$

where $a = l, r$ refers to left and right magnetic site in the M-O-M cluster as depicted in Fig. 1. Spin-orbit coupling is assumed to exist for the magnetic ions which are connected to the oxygen through the wave function overlap. The spins $\mathbf{S}_{a,b}$ in each of the three degenerate t_{2g} orbitals are subject to the local magnetic field along $\hat{m}_a = (\sin \theta_a \cos \phi_a, \sin \theta_a \sin \phi_a, \cos \theta_a)$. Ultimately such effective fields arise due to inter-atomic exchange interaction but also due to the strong Hund coupling within the individual magnetic ion. In such a case the strength of U mimicking the Hund coupling energy may well exceed the spin-orbit interaction strength λ . The large- U limit thus provides a natural starting point for the analysis of the spin-polarization coupling in the cluster model. In this section we propose a method that is particularly suited to treat the large U limit, namely $U \gg \lambda, V$ where V represents the M-O hybridization.

The overall Hamiltonian describing the three-atom cluster is given by $H = H_M + H_O + H_V$: H_M is already given in Eq. (1) and the other two terms, referring to the oxygen orbital and the M-O hybridization, are

$$\begin{aligned} H_O &= E_p \sum_{b=x,y,z} \sum_{\sigma} p_{b\sigma}^+ p_{b\sigma} \\ H_V &= V \sum_{\sigma} (d_{l,xy\sigma}^+ p_{y\sigma} + d_{l,zx\sigma}^+ p_{z\sigma} \\ &\quad - d_{r,xy\sigma}^+ p_{y\sigma} - d_{r,zx\sigma}^+ p_{z\sigma} + \text{h.c.}) \end{aligned}$$

(2)

Particle-hole transformations have been implemented on all three atomic sites¹⁰. The on-site energy of the oxygen atom, $-E_p$, becomes $+E_p$ after the transformation. The spin-orbit interaction, not included here, will be introduced later as a perturbation.

Now we discuss how one obtains a low-energy effective Hamiltonian from Eq. (2). First, due to the large energy difference $2U$ separating the spin-up (parallel to \hat{m}_a) and spin-down (antiparallel to \hat{m}_a) t_{2g} states, we can truncate the high-energy d -orbital states from the outset and write down the effective Hamiltonian using only the low-energy operators

$$\begin{aligned} d_{a,xy}^+ &= \cos \frac{\theta_a}{2} d_{a,xy\uparrow}^+ + e^{-i\phi_a} \sin \frac{\theta_a}{2} d_{a,xy\downarrow}^+ \\ d_{a,zx}^+ &= \cos \frac{\theta_a}{2} d_{a,zx\uparrow}^+ + e^{-i\phi_a} \sin \frac{\theta_a}{2} d_{a,zx\downarrow}^+ \end{aligned} \quad (3)$$

The d_{yz} orbital does not hybridize with any of the oxygen p -orbitals in the linear geometry we consider in this paper. This, and the p_x -orbital which does not hybridize with any of the d -orbitals, will be left out.

In this reduced Hilbert space the low-energy effective Hamiltonian becomes

$$\begin{aligned} H' &= H'_M + H'_O + H'_V \\ H'_M &= -U \sum_{a=l,r} (d_{a,xy}^+ d_{a,xy} + d_{a,zx}^+ d_{a,zx}) \\ H'_O &= E_p \sum_{\sigma} (p_{y\sigma}^+ p_{y\sigma} + p_{z\sigma}^+ p_{z\sigma}) \\ H'_V &= V (d_{l,xy}^+ p_{l,y} + d_{l,zx}^+ p_{l,z} \\ &\quad - d_{r,xy}^+ p_{r,y} - d_{r,zx}^+ p_{r,z} + \text{h.c.}) \end{aligned} \quad (4)$$

In writing down H'_V spin rotations similar to Eq. (3) have been employed also for the p -orbital operators:

$$\begin{aligned} p_{a,y}^+ &= \cos \frac{\theta_a}{2} p_{y\uparrow}^+ + e^{-i\phi_a} \sin \frac{\theta_a}{2} p_{y\downarrow}^+ \\ p_{a,z}^+ &= \cos \frac{\theta_a}{2} p_{z\uparrow}^+ + e^{-i\phi_a} \sin \frac{\theta_a}{2} p_{z\downarrow}^+ \end{aligned} \quad (5)$$

The axis of the three-atom cluster is taken as the $+\hat{x}$ axis going from left to right in Fig. 1. Until the spin-orbit coupling is introduced, the (d_{xy}, p_y) orbital pair remains decoupled from (d_{zx}, p_z) .

The p -orbital operators $(p_{l,y}, p_{r,y})$ are not orthogonal to each other. The same is true of $(p_{l,z}, p_{r,z})$. For further manipulation of the Hamiltonian we need to introduce a set of orthogonal operators

$$Y_1^+ = \frac{1}{\sqrt{2(1+|\kappa|)}} (p_{r,y}^+ + e^{i\eta} p_{l,y}^+)$$

$$\begin{aligned}
Y_2^+ &= \frac{1}{\sqrt{2(1-|\kappa|)}}(p_{r,y}^+ - e^{i\eta}p_{l,y}^+) \\
Z_1^+ &= \frac{1}{\sqrt{2(1+|\kappa|)}}(p_{r,z}^+ + e^{i\eta}p_{l,z}^+) \\
Z_2^+ &= \frac{1}{\sqrt{2(1-|\kappa|)}}(p_{r,z}^+ - e^{i\eta}p_{l,z}^+)
\end{aligned} \tag{6}$$

for the p -orbitals and

$$\begin{aligned}
D_{1,xy}^+ &= \frac{1}{\sqrt{2}}(-d_{r,xy}^+ + e^{i\eta}d_{l,xy}^+) \\
D_{2,xy}^+ &= \frac{1}{\sqrt{2}}(-d_{r,xy}^+ - e^{i\eta}d_{l,xy}^+) \\
D_{1,zx}^+ &= \frac{1}{\sqrt{2}}(-d_{r,zx}^+ + e^{i\eta}d_{l,zx}^+) \\
D_{2,zx}^+ &= \frac{1}{\sqrt{2}}(-d_{r,zx}^+ - e^{i\eta}d_{l,zx}^+)
\end{aligned} \tag{7}$$

for d -orbital states. We have defined $e^{i\eta} = \kappa/|\kappa|$ where

$$\begin{aligned}
\kappa &= \langle p_{l,y} | p_{r,y} \rangle = \langle p_{l,z} | p_{r,z} \rangle \\
&= \cos \frac{\theta_l}{2} \cos \frac{\theta_r}{2} + e^{i(\phi_l - \phi_r)} \sin \frac{\theta_l}{2} \sin \frac{\theta_r}{2}.
\end{aligned} \tag{8}$$

Using these new operators, the Hamiltonian in Eq. (4) becomes

$$\begin{aligned}
H &= H_Y + H_Z \\
H_Y &= - \sum_{\alpha=1,2} (D_{\alpha,xy}^+ \ Y_{\alpha}^+) \mathcal{H}_{\alpha} \begin{pmatrix} D_{\alpha,xy} \\ Y_{\alpha} \end{pmatrix} \\
H_Z &= - \sum_{\alpha=1,2} (D_{\alpha,zx}^+ \ Z_{\alpha}^+) \mathcal{H}_{\alpha} \begin{pmatrix} D_{\alpha,zx} \\ Z_{\alpha} \end{pmatrix} \\
\mathcal{H}_{\alpha} &= E_0 + E_{\alpha} \begin{pmatrix} \cos \beta_{\alpha} & -\sin \beta_{\alpha} \\ -\sin \beta_{\alpha} & -\cos \beta_{\alpha} \end{pmatrix}
\end{aligned} \tag{9}$$

with $E_0 = (U - E_p)/2$, $E_{\alpha} = \sqrt{(U + E_p)^2/4 + V_{\alpha}^2}$, and $V_{1,2} = V\sqrt{1 \pm |\kappa|}$, $(\cos \beta_{\alpha}, \sin \beta_{\alpha}) = ((U + E_p)/2E_{\alpha}, V_{\alpha}/E_{\alpha})$. H_Y and H_Z can be diagonalized through the rotation

$$\begin{aligned}
\begin{pmatrix} D_{\alpha,xy} \\ Y_{\alpha} \end{pmatrix} &= \begin{pmatrix} -\cos \beta_{\alpha}/2 & \sin \beta_{\alpha}/2 \\ \sin \beta_{\alpha}/2 & \cos \beta_{\alpha}/2 \end{pmatrix} \begin{pmatrix} \psi_{\alpha} \\ \varphi_{\alpha} \end{pmatrix} \\
\begin{pmatrix} D_{\alpha,zx} \\ Z_{\alpha} \end{pmatrix} &= \begin{pmatrix} -\cos \beta_{\alpha}/2 & \sin \beta_{\alpha}/2 \\ \sin \beta_{\alpha}/2 & \cos \beta_{\alpha}/2 \end{pmatrix} \begin{pmatrix} \psi'_{\alpha} \\ \varphi'_{\alpha} \end{pmatrix}
\end{aligned} \tag{10}$$

into

$$\begin{aligned}
H_Y &= \sum_{\alpha} -(E_0 + E_{\alpha})\psi_{\alpha}^+ \psi_{\alpha} + \sum_{\alpha} (E_{\alpha} - E_0)\varphi_{\alpha}^+ \varphi_{\alpha}, \\
H_Z &= \sum_{\alpha} -(E_0 + E_{\alpha})\psi'_{\alpha}^+ \psi'_{\alpha} + \sum_{\alpha} (E_{\alpha} - E_0)\varphi'_{\alpha}^+ \varphi'_{\alpha}.
\end{aligned} \tag{11}$$

Four degenerate levels $(\psi_1, \psi_2, \psi'_1, \psi'_2)$ are separated from the other four degenerate set $(\varphi_1, \varphi_2, \varphi'_1, \varphi'_2)$ with an energy spacing of nearly $U + E_p$. This large energy separation sets the stage for introducing spin-orbit interaction $H_{SO} = \lambda S \cdot L$ within each of the four-dimensional manifolds, but not between the two manifolds. We obtain the effective Hamiltonian valid within each manifold,

$$\begin{aligned}
\mathcal{H} &= \begin{pmatrix} \psi_1^+ \\ \psi_2^+ \\ \psi'_1^+ \\ \psi'_2^+ \end{pmatrix}^T \begin{pmatrix} -U_1 & 0 & -i\lambda_1 & -i\lambda_2 \\ 0 & -U_2 & -i\lambda_2 & -i\lambda_3 \\ i\lambda_1 & i\lambda_2 & -U_1 & 0 \\ i\lambda_2 & i\lambda_3 & 0 & -U_2 \end{pmatrix} \begin{pmatrix} \psi_1 \\ \psi_2 \\ \psi'_1 \\ \psi'_2 \end{pmatrix} \\
&+ \begin{pmatrix} \varphi_1^+ \\ \varphi_2^+ \\ \varphi'_1^+ \\ \varphi'_2^+ \end{pmatrix}^T \begin{pmatrix} E_1^p & 0 & -i\lambda'_1 & -i\lambda'_2 \\ 0 & E_2^p & -i\lambda'_2 & -i\lambda'_3 \\ i\lambda'_1 & i\lambda'_2 & E_1^p & 0 \\ i\lambda'_2 & i\lambda'_3 & 0 & E_2^p \end{pmatrix} \begin{pmatrix} \varphi_1 \\ \varphi_2 \\ \varphi'_1 \\ \varphi'_2 \end{pmatrix}
\end{aligned} \tag{12}$$

where $U_{\alpha} = E_0 + E_{\alpha}$, $E_{\alpha}^p = E_{\alpha} - E_0$, and

$$\begin{aligned}
i\lambda_1 &= \langle \psi'_1 | H_{SO} | \psi_1 \rangle = \frac{i\lambda}{2} \cos^2 \frac{\beta_1}{2} (m_r^x + m_l^x) \\
i\lambda_2 &= \langle \psi'_1 | H_{SO} | \psi_2 \rangle = \langle \psi_2 | H_{SO} | \psi'_1 \rangle \\
&= \frac{i\lambda}{2} \cos \frac{\beta_1}{2} \cos \frac{\beta_2}{2} (m_r^x - m_l^x) \\
i\lambda_3 &= \langle \psi'_2 | H_{SO} | \psi_2 \rangle = \frac{i\lambda}{2} \cos^2 \frac{\beta_2}{2} (m_r^x + m_l^x) \\
i\lambda'_1 &= \langle \varphi'_1 | H_{SO} | \varphi_1 \rangle = \frac{i\lambda}{2} \sin^2 \frac{\beta_1}{2} (m_r^x + m_l^x) \\
i\lambda'_2 &= \langle \varphi'_1 | H_{SO} | \varphi_2 \rangle = \langle \varphi_2 | H_{SO} | \varphi'_1 \rangle \\
&= \frac{i\lambda}{2} \sin \frac{\beta_1}{2} \sin \frac{\beta_2}{2} (m_r^x - m_l^x) \\
i\lambda'_3 &= \langle \varphi'_2 | H_{SO} | \varphi_2 \rangle = \frac{i\lambda}{2} \sin^2 \frac{\beta_2}{2} (m_r^x + m_l^x).
\end{aligned} \tag{13}$$

Here m_a^x refers to the x -component of the local quantization axis for left and right magnetic sites. Because of small V/U , we can safely take

$$\begin{aligned}
E_1 &= E_2 = E = (U + E_p)/2 \\
\cos \beta_{\alpha}/2 &\approx 1 \\
\sin \beta_{\alpha}/2 &\approx V_{\alpha}/(U + E_p)
\end{aligned} \tag{14}$$

in Eq. (13). The above Hamiltonian \mathcal{H} can be diagonalized to the form

$$\mathcal{H} = \sum_{i=1}^4 E_i^L \cdot \Psi_i^+ \Psi_i + \sum_{i=1}^4 E_i^H \cdot \Phi_i^+ \Phi_i \tag{15}$$

with the eigen-states

$$\begin{aligned}
\Psi_i &= \xi_1^i \psi_1 + \xi_2^i \psi_2 + \xi_3^i \psi'_1 + \xi_4^i \psi'_2 \\
\Phi_i &= \zeta_1^i \varphi_1 + \zeta_2^i \varphi_2 + \zeta_3^i \varphi'_1 + \zeta_4^i \varphi'_2.
\end{aligned} \tag{16}$$

One can verify that the coefficients satisfy

$$\begin{aligned} |\xi_1^i| &= |\xi_3^i|, \quad |\xi_2^i| = |\xi_4^i|, \quad \bar{\xi}_1^i \xi_2^i = \bar{\xi}_3^i \xi_4^i \in \text{Re} \\ |\zeta_1^i| &= |\zeta_3^i|, \quad |\zeta_2^i| = |\zeta_4^i|, \quad \bar{\zeta}_1^i \zeta_2^i = \bar{\zeta}_3^i \zeta_4^i \in \text{Re}. \end{aligned} \quad (17)$$

This completes the formal derivation of the full set of eigenstates in the limit $U \gg \lambda, V$. The remaining task is to calculate the polarization $\langle \mathbf{r} \rangle$ for each of the eigenstates obtained.

Due to the shapes of d - and p -orbitals, only the following overlap integrals are non-zero ($\mathbf{x} = x\hat{x}$):

$$\begin{aligned} \langle d_{r,xy\sigma} | \mathbf{x} | p_{y\sigma} \rangle &= \langle d_{l,xy\sigma} | \mathbf{x} | p_{y\sigma} \rangle \\ &= \langle d_{r,zx\sigma} | \mathbf{x} | p_{z\sigma} \rangle = \langle d_{l,zx\sigma} | \mathbf{x} | p_{z\sigma} \rangle = L\hat{x}. \end{aligned} \quad (18)$$

Here $L = \int d^3\mathbf{r} d_{i,xy\sigma}(\mathbf{r}) \mathbf{x} p_{y\sigma}(\mathbf{r})$ ($i = r, l$). If non-zero polarization develops, it can only be in the \hat{x} direction, i.e. along the axis of the three-atom cluster, within the lowest order in λ/Δ , $\Delta = U + E_p$. Note that the transverse component obtained in Ref. 10 corresponds to the terms of the first order in λ/Δ . This contribution is numerically studied later in Sec. III. For clarity of the presentation we show the diagonal and off-diagonal contributions to the polarization separately.

Diagonal terms: Since

$$\langle Y_1 | \mathbf{r} | D_{1,xy} \rangle = \frac{L}{2\sqrt{1+|\kappa|}} [1 - 1 + |\kappa| - |\kappa|] \hat{x} = 0, \quad (19)$$

we have

$$\begin{aligned} \langle \psi_1 | \mathbf{r} | \psi_1 \rangle &= -\frac{\sin \beta_1}{2} [\langle D_{1,xy} | \mathbf{r} | Y_1 \rangle + \langle Y_1 | \mathbf{r} | D_{1,xy} \rangle] = 0, \\ \langle \varphi_1 | \mathbf{r} | \varphi_1 \rangle &= \frac{\sin \beta_1}{2} [\langle D_{1,xy} | \mathbf{r} | Y_1 \rangle + \langle Y_1 | \mathbf{r} | D_{1,xy} \rangle] = 0. \end{aligned} \quad (20)$$

All other diagonal terms vanish as well, $\langle \psi_m | \mathbf{r} | \psi_m \rangle = \langle \psi'_m | \mathbf{r} | \psi'_m \rangle = \langle \varphi_m | \mathbf{r} | \varphi_m \rangle = \langle \varphi'_m | \mathbf{r} | \varphi'_m \rangle = 0$.

Off-diagonal terms: In view of the symmetry of the orbital overlaps given in Eq. (18), the following averages must be zero: $\langle \psi_1 | \mathbf{r} | \psi'_1 \rangle = \langle \psi_1 | \mathbf{r} | \psi'_2 \rangle = \langle \psi_2 | \mathbf{r} | \psi'_1 \rangle = \langle \psi_2 | \mathbf{r} | \psi'_2 \rangle = 0$. Thus, only $\langle \psi_1 | \mathbf{r} | \psi_2 \rangle$, $\langle \psi'_1 | \mathbf{r} | \psi'_2 \rangle$ and $\langle \varphi_1 | \mathbf{r} | \varphi_2 \rangle$, $\langle \varphi'_1 | \mathbf{r} | \varphi'_2 \rangle$ may contribute to the polarization. Since

$$\begin{aligned} \langle D_{1,xy} | \mathbf{r} | Y_2 \rangle &= -\hat{x} \times L \sqrt{1-|\kappa|} \\ \langle Y_1 | \mathbf{r} | D_{2,xy} \rangle &= -\hat{x} \times L \sqrt{1+|\kappa|}, \end{aligned} \quad (21)$$

we have

$$\begin{aligned} \langle \psi_1 | \mathbf{r} | \psi_2 \rangle &= \\ &- \cos \frac{\beta_1}{2} \sin \frac{\beta_2}{2} \langle D_{1,xy} | \mathbf{r} | Y_2 \rangle - \sin \frac{\beta_1}{2} \cos \frac{\beta_2}{2} \langle Y_1 | \mathbf{r} | D_{2,xy} \rangle \\ &\simeq \hat{x} \times \frac{LV}{\Delta} [(1 - |\kappa|) + (1 + |\kappa|)] = \hat{x} \times \frac{2LV}{\Delta}, \end{aligned}$$

$$\begin{aligned} \langle \varphi_1 | \mathbf{r} | \varphi_2 \rangle &= \\ &\sin \frac{\beta_1}{2} \cos \frac{\beta_2}{2} \langle D_{1,xy} | \mathbf{r} | Y_2 \rangle + \cos \frac{\beta_1}{2} \sin \frac{\beta_2}{2} \langle Y_1 | \mathbf{r} | D_{2,xy} \rangle \\ &\simeq -\hat{x} \times \frac{2LV}{\Delta} \sqrt{1-|\kappa|^2} = -\hat{x} \times \frac{\sqrt{2}LV}{\Delta} \sqrt{1-\sigma_1 \cdot \sigma_2}. \end{aligned} \quad (22)$$

Similarly,

$$\begin{aligned} \langle D_{1,zx} | \mathbf{r} | Z_2 \rangle &= -\hat{x} \times L \sqrt{1-|\kappa|} \\ \langle Z_1 | \mathbf{r} | D_{2,zx} \rangle &= -\hat{x} \times L \sqrt{1+|\kappa|} \end{aligned} \quad (23)$$

gives

$$\begin{aligned} \langle \psi'_1 | \mathbf{r} | \psi'_2 \rangle &= \\ &- \cos \frac{\beta_1}{2} \sin \frac{\beta_2}{2} \langle D_{1,zx} | \mathbf{r} | Z_2 \rangle - \sin \frac{\beta_1}{2} \cos \frac{\beta_2}{2} \langle Z_1 | \mathbf{r} | D_{2,zx} \rangle \\ &\simeq \hat{x} \times \frac{2LV}{\Delta}, \end{aligned}$$

$$\begin{aligned} \langle \varphi'_1 | \mathbf{r} | \varphi'_2 \rangle &= \\ &\sin \frac{\beta_1}{2} \cos \frac{\beta_2}{2} \langle D_{1,zx} | \mathbf{r} | Z_2 \rangle + \cos \frac{\beta_1}{2} \sin \frac{\beta_2}{2} \langle Z_1 | \mathbf{r} | D_{2,zx} \rangle \\ &\simeq -\hat{x} \times \frac{\sqrt{2}LV}{\Delta} \sqrt{1-\sigma_1 \cdot \sigma_2}. \end{aligned} \quad (24)$$

Based on the above calculations, the final expression for the polarization \mathbf{P} reads

$$\begin{aligned} \mathbf{P}_{\Psi_i} &= \langle \Psi_i | \mathbf{r} | \Psi_i \rangle = 2\bar{\xi}_1^i \xi_2^i [\langle \psi_1 | \mathbf{r} | \psi_2 \rangle + \langle \psi'_1 | \mathbf{r} | \psi'_2 \rangle] \\ &\approx \hat{x} \times \frac{8\bar{\xi}_1^i \xi_2^i LV}{\Delta}, \\ \mathbf{P}_{\Phi_i} &= \langle \Phi_i | \mathbf{r} | \Phi_i \rangle = \frac{1}{2} \bar{\zeta}_1^i \zeta_2^i [\langle \varphi_1 | \mathbf{r} | \varphi_2 \rangle + \langle \varphi'_1 | \mathbf{r} | \varphi'_2 \rangle] \\ &\approx -\hat{x} \times \frac{\sqrt{2}\bar{\zeta}_1^i \zeta_2^i LV}{\Delta} \sqrt{1-\sigma_1 \cdot \sigma_2}. \end{aligned} \quad (25)$$

Note that $\bar{\xi}_1^i \xi_2^i$ and $\bar{\zeta}_1^i \zeta_2^i$ are also dependent on the spin configuration. The full spin dependence of the polarization may be rather complicated. However, because of small V/U , we can take $U_1 = U_2 = U$ and

$$\begin{aligned} \lambda_1 &= \lambda_3 = \frac{\lambda}{2} (m_l^x + m_r^x) \\ \lambda_2 &= \frac{\lambda}{2} (m_r^x - m_l^x). \end{aligned} \quad (26)$$

Under such an approximation the low-energy eigenstates are given by the surprisingly simple form

$$\begin{aligned}\Psi_1 &= (i\psi_1 + i\psi_2 + \psi'_1 + \psi'_2)/2, & E_1^L &= -U - \lambda_1 - \lambda_2 \\ \Psi_2 &= (i\psi_1 - i\psi_2 - \psi'_1 + \psi'_2)/2, & E_2^L &= -U + \lambda_1 - \lambda_2 \\ \Psi_3 &= (-i\psi_1 + i\psi_2 - \psi'_1 + \psi'_2)/2, & E_3^L &= -U - \lambda_1 + \lambda_2 \\ \Psi_4 &= (-i\psi_1 - i\psi_2 + \psi'_1 + \psi'_2)/2, & E_4^L &= -U + \lambda_1 + \lambda_2.\end{aligned}\quad (27)$$

For each of the eigenstates above the polarization \mathbf{P}_{Ψ_i} reads

$$\begin{aligned}\mathbf{P}_{\Psi_1} &= \mathbf{P}_{\Psi_4} = \hat{x} \times \frac{2LV}{\Delta} \\ \mathbf{P}_{\Psi_2} &= \mathbf{P}_{\Psi_3} = -\hat{x} \times \frac{2LV}{\Delta}.\end{aligned}\quad (28)$$

The polarization, constant in magnitude but reversible in sign, is developed along the M-O-M cluster. Since λ_1 and λ_2 depend on the spin directions and in particular on m_l^x and m_r^x as shown in Eq. (26), which one of the four states shown in Eq. (27) becomes the true ground state depends on the set of values (m_l^x, m_r^x) . In Fig. 2 we map out the polarization directions of the ground state for all the available situations within the zeroth order in λ/Δ . The reversal of the polarization direction occurs whenever $|m_l^x| = |m_r^x|$ line is crossed. The sudden change of the sign is due to level crossing of the two eigenstates when λ_1 or λ_2 vanishes at $|m_l^x| = |m_r^x|$. The ground state polarization is consistent with the functional form $P_x \sim (m_r^x)^2 - (m_l^x)^2$.

If a single hole is introduced in the cluster, the polarization is given by one of the expressions in Eq. (28). With two holes, two opposite polarizations from Eq. (28) cancel out to produce $\mathbf{P} = 0$. In the numerical results presented in the next section, however, one finds a finite longitudinal polarization even for the two-hole case because of the higher-order terms in λ/Δ , and the polarization direction is still dictated by $P_x \sim (m_r^x)^2 - (m_l^x)^2$.

III. NUMERICAL RESULTS

The results of the previous section gave the electronic polarization solely along the axis of the atomic cluster. In the analysis it was assumed that the large effective Zeeman energy U dominates over both the spin-orbit interaction λ and the hybridization amplitude V . It was also assumed that d_{yz} and p_x orbitals did not play a role. According to Ref. 10, on the other hand, transverse polarization such as P_y can only arise from the overlap integral $\langle d_{yz}|y|p_z\rangle$ or $\langle d_{xy}|y|p_x\rangle$. In the numerical approach this condition can be relaxed and indeed we find non-zero transverse polarization as well as the longitudinal polarization in accordance with the theory presented in the previous section. In general the results

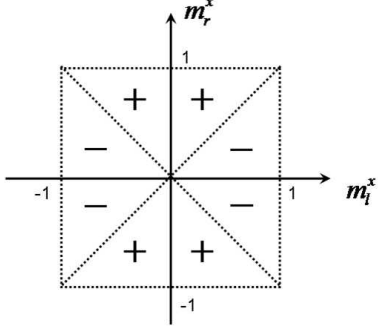


FIG. 2: The direction of longitudinal polarization $P_x = \mathbf{P} \cdot \hat{x}$ in the ground state wave function plotted for (m_l^x, m_r^x) , $-1 \leq m_l^x, m_r^x \leq 1$. $(+/-)$ refers to $P_x > (<) 0$. P_x is indeterminate along two dotted lines ($m_l^x = m_r^x$ and $m_l^x = -m_r^x$) due to the level crossing occurring along these lines.

depend sensitively on the number of holes inserted in the cluster, with the even and odd number of holes yielding different behavior. As a representative case for each, we consider one- and two-hole situations in detail. When extrapolated to the infinite lattice they correspond to the metallic and insulating cases, respectively.

The Hilbert space for the single-particle mean-field Hamiltonian is 18-dimensional, consisting of Eq. (1) and Eq. (2), with six from each atomic site. In practice, one can treat the 16-dimensional problem leaving out the oxygen p_x orbital without loss of generality, since it remains decoupled from the rest of the atomic states in the exact solution.

A. One hole (double-exchange interaction)

The polarization $\langle \mathbf{r} \rangle$ is calculated with respect to the lowest-energy eigenstate of the particle-hole transformed Hamiltonian corresponding to putting one hole in the cluster. For ease of presentation we restrict ourselves to situations where both spins lie in the XY plane: $\hat{m}_l = (\cos \phi_l, \sin \phi_l, 0)$, $\hat{m}_r = (\cos \phi_r, \sin \phi_r, 0)$. The resulting longitudinal polarization P_x is plotted as a function of (ϕ_l, ϕ_r) in Fig. 3. The similarity between the numerically obtained P_x and the predicted behavior $P_x \sim \cos 2\phi_r - \cos 2\phi_l$ is striking. The magnitude of the polarization, according to Eq. (28) and using the parameters used in the numerical study, is expected to be $|P_x| \sim 0.05L$, in good agreement with the numerical results.

In addition, we find non-zero P_y in the numerical calculation due to the inclusion of d_{yz} orbital. The behavior of P_y we find is consistent with the directional dependence $P_y \sim \text{sgn}[\cos(\Delta\phi/2)] \sin(\Delta\phi/2)$ ($\Delta\phi = \phi_r - \phi_l$) expected in Ref. 10 (See Eq. (4) in Ref. 10). Also the order of magnitude $|P_y| \sim 0.01L$ obtained numerically is consistent with Ref. 10. P_z vanishes for the two spins lying in the XY plane, as shown both analytically and numerically.

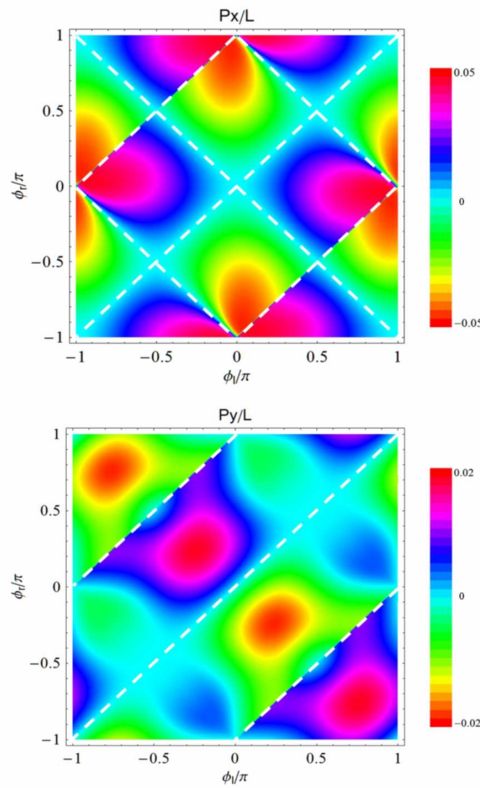


FIG. 3: (color online) The calculated polarization P_x and P_y from exact diagonalization of the full M-O-M cluster Hamiltonian with a single hole. Dotted white lines indicate P_x or P_y equal to zero. P_x vanishes not only when the spins are collinear, but also when $\phi_l + \phi_r = \pm\pi$, as discussed in Sec. II. The overall directional dependence for P_x is consistent with $\cos 2\phi_r - \cos 2\phi_l$. The sharp change in the sign of P_x along $\phi_r = \phi_l \pm \pi$ lines is due to the energy level crossing in the ground state. P_x turns to zero along the lines (indicated as dotted white lines) where the spins become collinear. The parameters used in this calculation are $(U/V, E_p/V, \lambda/V) = (10, 30, 0.3)$.

B. Two holes (superexchange interaction)

When two holes are introduced in the cluster, the ground state can be changed adiabatically without a level crossing as the two spin directions are varied, and hence the polarization exhibits a smooth change. Typical numerical results for the longitudinal and transverse components of the polarization are shown in the upper and lower panels of Fig. 4. As in the previous consideration for one hole, the spin directions are varied within the XY plane with $\hat{m}_l = (\cos \phi_l, \sin \phi_l, 0)$ and $\hat{m}_r = (\cos \phi_r, \sin \phi_r, 0)$.

We analyzed the directional dependence of the polarization by using the following forms:

$$P_x/L = A [\cos(2\phi_r) - \cos(2\phi_l)]$$

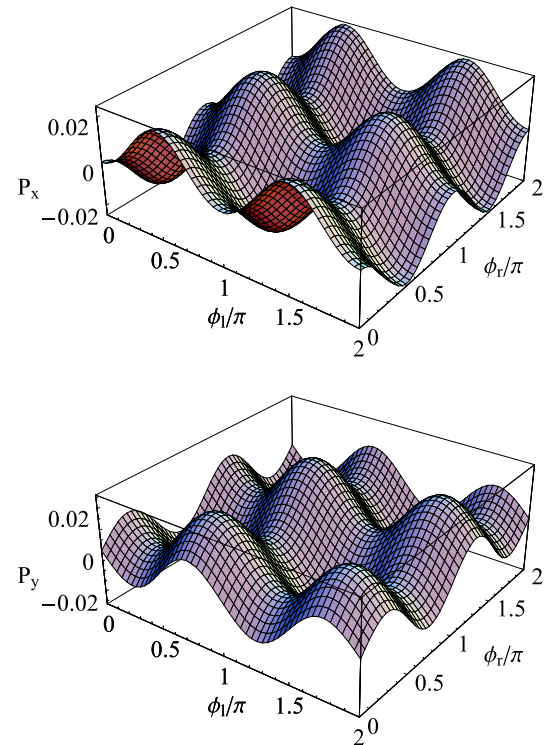


FIG. 4: (color online) Induced polarization P_x and P_y in a unit of L for the superexchange case with two holes in the three-atom cluster. The parameters used in this calculation are the same as in Fig. 3.

$$P_y/L = -B_1 \sin(\phi_r - \phi_l) + B_2 [\sin(2\phi_r) - \sin(2\phi_l)]. \quad (29)$$

While the least-square fit to the numerical results were made using as many as six different basis functions, only those listed above made a sizable contribution. The angle dependence of the transverse polarization P_y predicted in Ref. 10 corresponds to the $B_1 \sin(\phi_r - \phi_l)$ term above, whereas the angle dependence of P_x is consistent with the single-hole results analytically derived in the previous section. The second term in P_y , proportional to B_2 , was not anticipated in analytic theories but show up in the numerical analysis. In the spiral phase for the spins, $B_1 \sin(\phi_r - \phi_l)$ produces a uniform transverse component while all other terms give rise to a macroscopically vanishing polarization. In this regard the new terms (A and B_2) correspond to “oscillating” component of the polarization in contrast to the uniform component given by B_1 .

Shown in Fig. 5 are the coefficients, A , B_1 , and B_2 , for a wide range of parameters, $0 \leq \lambda/V \leq 10$, $0 \leq U/V \leq 10$, obtained by fitting the numerical data using Eq. (29). Several features are worth mentioning: (i) A and B_2 are remarkably similar over most of the parameter space. This implies that the non-uniform polarization develops with similar magnitudes along and orthogonal to the bond axis. (ii) Large non-uniform po-

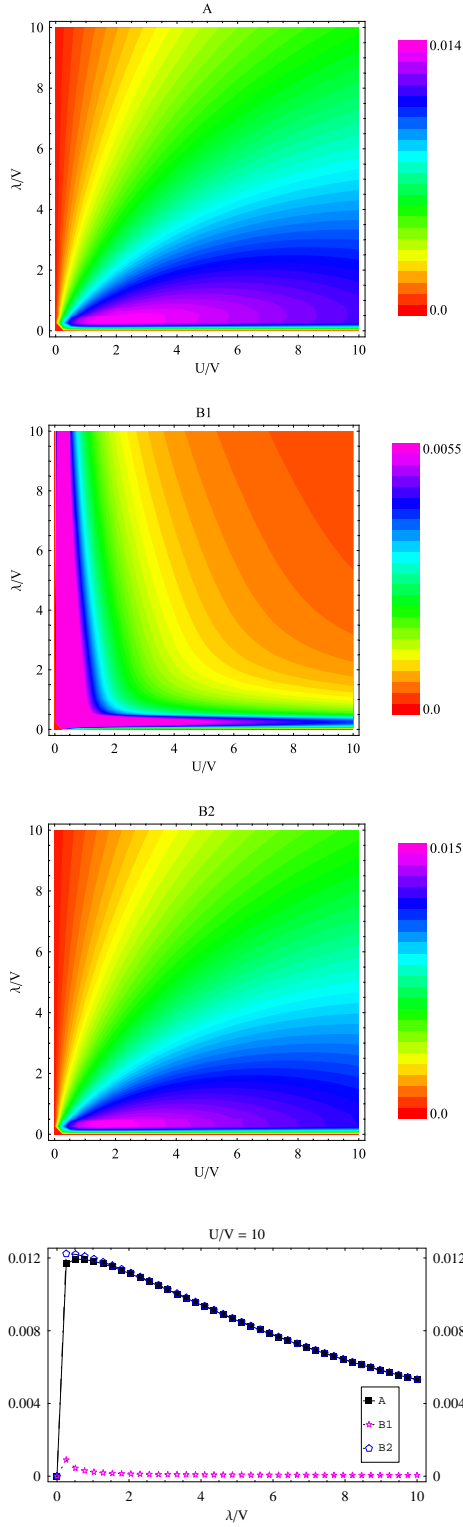


FIG. 5: (color online) (top three figures) Fourier components A , B_1 , and B_2 , in the polarization P_x/L and P_y/L using the fitting formula, Eq. (29). (bottom) Fourier components with $U/V = 10$ and varying λ/V .

larization components are attained for large U/V and

small λ/V as indicated by the blue and violet regions in Fig. 5. On the other hand, large uniform polarization (B_1) is achieved for large λ/V and small U/V in agreement with Ref. 10, where $\lambda \gtrsim U$ was implicitly assumed. To be concrete, the largest values for A , B_1 and B_2 are obtained for $(U/V, \lambda/V) = (1.795, 0.256)$, $(0.256, 0.256)$, and $(1.794, 0.256)$ respectively, with the magnitudes indicated on the vertical bar next to each figure. Using an earlier estimate¹⁰, these maximal values correspond to $A \sim B_2 \sim 2 \times 10^2 \text{ nC/cm}^2$ and $B_1 \sim 80 \text{ nC/cm}^2$. For U/V large, the polarization mainly possesses the oscillating components with a much smaller uniform component as explicitly demonstrated at the bottom of Fig. 5 for U/V fixed at a large value ($U/V = 10$) and varying λ/V .

The macroscopic polarization is governed by the B_1 term alone. On the other hand, the Fourier analysis reveals the local magnitudes of the oscillating component to be much larger than the uniform polarization over most of the parameter ranges, increasing the chance to observe coupling of the local dipole order to external probes such as X-ray or neutron scattering. Particularly in spiral magnets with ordering wavevector \mathbf{Q} , the oscillation of electric dipole moments appears with the wavevector $2\mathbf{Q}$, since we have found that the nonuniform part has the form $\sin 2\phi_l - \sin 2\phi_r$ for the transverse component and $\cos 2\phi_l - \cos 2\phi_r$ for the longitudinal one. Figure 6 shows the simplest example with the periodicity of the eight M ions where relative angles between the neighboring spins are $\pi/4$. In this case, electric dipole moments induced at oxygen ions also rotate with half the magnetic periodicity. Note that the amplitude of this nonuniform part is much larger than the uniform part. It is expected that oxygen ions subject to such electric dipole field shift in either parallel or anti-parallel directions to the local dipole moment.

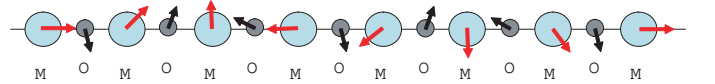


FIG. 6: Spiral spin structure (red arrows) with an angle shift of $\pi/4$ between neighboring magnetic (M) ions and the induced dipole moments (parallel or anti-parallel to black arrows) at oxygen (O) sites with half the periodicity. Uniform component is not shown since it is much smaller than the nonuniform part.

IV. DISCUSSION

In this paper we have developed a theory for the spin-induced electric polarization in a simple three-atom cluster model proposed in Ref. 10. The truncation to the low-energy space is allowed by the large energy separation between spin-up and spin-down states of the magnetic site due to the strong effective Zeeman field, and the much smaller energy scale for the pd -hybridization

V and spin-orbit interaction λ . The net electric dipole moment is found to be along the cluster's axis within our approximation, and the numerical calculation confirmed this conclusion. The longitudinal polarization has an oscillating character, and vanishes in the macroscopic limit. Numerical analysis further identified uniform and non-uniform components in the transverse polarization. The magnitude of the non-uniform transverse polarization is comparable to the non-uniform longitudinal one. Such non-uniform polarizations generically have larger magnitudes on the atomic scale than the uniform transverse component.

To this date, all experimental works of spin-induced polarization have reported only the macroscopic polarization perpendicular to the spin modulation vector^{1–4,6,7}. More detailed studies on X-ray and neutron scattering experiments^{4–6} are desired to detect the non-uniform polarization associated with non-collinear magnetic structures.

On the theory side, a Ginzburg-Landau consideration led to the conclusion that the uniform polarization direction is orthogonal to the modulation wavevector of the spin^{8,9}. In Ref. 8 some non-uniform components of the polarization is predicted on the basis of Ginzburg-Landau theory without a detailed discussion of its implications. Furthermore, consideration of the orbital structure for the magnetic site is missing in the phenomenological the-

ories advanced so far. For instance, the t_{2g} levels alone break the rotational symmetry in the orbital space and the corresponding Ginzburg-Landau theory need not possess the invariance under spatial rotation. It will be interesting to develop a Ginzburg-Landau theory with a proper symmetry consideration for the t_{2g} systems to see if the new features we observe, i.e. non-uniform longitudinal and transverse polarizations, emerge naturally.

Our results may also open up a possibility for a nanoscale device of switching the polarization by means of an applied magnetic field or the magnetization by means of an applied electric field. The so-called “quantum magnet” might be a candidate to such systems. The present results even pave a way to fabricate crystalline magnets, ferroelectrics and multiferroics having the longitudinal polarization.

Acknowledgments

The authors thank T. Arima for fruitful discussions. One of us (C. Jia) was supported by the Postdoctoral Research Program of Sungkyunkwan University (2006). The work was partly supported by Grant-in-Aids and NAREGI Nanoscience Project from the Ministry of Education, Culture, Sports, Science, and Technology.

* To whom correspondence should be addressed. Electronic address: hanjh@skku.edu

¹ T. Kimura *et al.* Nature **426**, 55 (2003).

² N. Hur *et al.* Nature **429**, 392 (2004).

³ G. Lawes *et al.* Phys. Rev. Lett. **95**, 087205 (2005).

⁴ M. Kenzelmann *et al.* Phys. Rev. Lett. **95**, 087206 (2005).

⁵ T. Arima *et al.* Phys. Rev. B **72**, 100102(R) (2005).

⁶ T. Arima *et al.* Phys. Rev. Lett. **96**, 07202 (2006).

⁷ Y. Yamasaki *et al.* Phys. Rev. Lett. **96**, 207204 (2006).

⁸ Maxim Mostovoy, Phys. Rev. Lett. **96**, 067601 (2006).

⁹ A. B. Harris and G. Lawes, cond-mat/0508617; A. B. Harris, cond-mat/0508730; A. B. Harris, T. Yildirim, A. Aharony, and O. Entin-Wohlman, cond-mat/0510807.

¹⁰ Hosho Katsura, Naoto Nagaosa, and Alexander V. Balatsky, Phys. Rev. Lett. **95**, 057205 (2005).

¹¹ I. A. Sergienko and E. Dagotto, Phys. Rev. B **73**, 094434 (2006).